KSCE Journal of Civil Engineering (2019) 23(7):3239-3249

DOI 10.1007/s12205-019-0172-5

Tunnel Engineering

pISSN 1226-7988, eISSN 1976-3808
www.springer.com/12205

Influence of Water on the Fracture Process of Marble with Acoustic Emission Monitoring

Jun Zhu*, Jianhui Deng, Yiming Huang***, and Zhiliang He******

Received February 16, 2019/Revised April 18, 2019/Accepted April 21, 2019/Published Online June 5, 2019

Abstract

Water has a great influence on rock fracture process, and it is necessary to explore the activity of cracks for saturated rocks at key stress points. By uniaxial compression test and acoustic emission (AE) tests, four key points of stress-strain curve for dry and saturated marble specimens are determined. Those four key stress points include: crack closure stress (point *A*), crack initiation stress (point *B*), crack damage stress (point *C*) and peak stress (point *D*). By analyzing dominant frequencies and amplitude of AE waveforms of the whole loading process and in the vicinity of key points, the fracture process of samples was studied. The results show that there are two concentrations of dominant frequency bands in both dry and saturated marble, and the ranges of dominant frequency bands of the saturated seem wider. Due to the existence of water, the number and energy of AE waveforms decrease relatively during the whole test. This phenomenon indicates that water enhances the ductility and creep characteristics of rock. The appearance of lots of AE waveform signals with low dominant frequency is the precursor information of intense crack propagation and failure for dry rock, and the effects of water increased the number of micro-tensile failures for saturated rock in the vicinity of each key point. From point *A*, point *B*, point *C* to point *D*, the proportions of H-type bands in the vicinity of each key point for dry rock show a trend of increasing - decreasing - sharply decreasing, while those for saturated rock follow the law of increasing - decreasing - increasing.

Keywords: *saturated, volumetric strain (crack volumetric strain), acoustic emission (AE), statistical analysis, dominant frequency*

1. Introduction

Rock mass in engineering is mostly in the water environment and often in the saturated state. Moisture in the rock can affect the long-term stability and safety of project (Fig. 1(a)). It is generally believed that properties of strength and deformation for rocks deteriorate after saturation (Hawkins and Mcconnell, 1992; Erguler and Ulusay, 2009; Yilmaz, 2010; Xiong *et al.*, 2011). In addition, rock mass will be relatively dry prior to the construction engineering, such as hydropower station (Fig. 1(b)). Rock is a brittle material with complex structure, and its failure process is essentially a macroscopic result of expansion, convergence and continuous development of internal cracks (Zhu *et al.*, 2015; Wu, 2018; Zhou *et al.*, 2016, 2017). Therefore, studying crack propagation in dry and saturated rocks is highly worthwhile to address of engineering problems.

The methods of previous research on crack propagation for rock mainly include two aspects: 1) numerical constitutive simulations (Areias *et al.*, 2015, 2018; Zhang *et al.*, 2015, 2018; Rabczuk *et al.*, 2007; Ren *et al.*, 2016), 2) experimental measurement from micro perspective, such as CT, high-speed video and so on. Specially, to describe the destruction characteristics of rocks essentially, AE technology is widely employed to the research of crack propagation (Rodríguez *et al.*, 2016; Wang *et al.*, 2018). The AE (acoustic emission) method includes parameter and waveform analysis, and plenty of information can be obtained from AE waveforms, such as stress state, microstructure, physical and mechanical properties of rocks (Cai *et al.*, 2007b; Lu *et a.l*, 2012).

Previous studies on the properties of crack propagation using AE method for saturated rocks covered the following aspects. AE and volumetric strain were employed by Eberhardt *et al*. (1998) to study the effect of water on crack propagation in brittle rocks. Khazaei *et al*. (2015) analyzed AE parameter of b-value and defined the propagation of the fracture planes. FFT method on AE waveform signals during the entire uniaxial compression process of sandstone was performed by Zhang *et al*. (2013). Xu *et al*. (2012) discussed the relationship between evolution law of

*Ph.D. Student, College of Water Resources and Hydropower, State Key Laboratory of Hydraulics and Mountain River Engineering, Sichuan University, Chengdu, Sichuan 610065, China (E-mail: scujun0305@163.com)
**Professor, College of Water Resources and Hydropower, State Key Laboratory of Hydraulics and Mountain River Engineering, Sichuan University, Chengdu, Sichuan 610065, China (Corresponding Author, E-mail: jhdeng@scu.edu.cn)
***Ph.D. Student, College of Water Resources and Hydropower, State Key Laboratory of Hydraulics and Mountain River Engineering, Sichuan University, Chengdu, Sichuan 610065, China (E-mail: chinasdhym@163.com)
****Ph.D. Student, Institute for Disaster Management and Reconstruction, Sichuan University, Chengdu, Sichuan 610065, China (E-mail: hzlscmy@outlook.com)

Fig. 1. Rock Mass in Dry and Saturated Condition: (a) Example of Jinping Hydropower Station in Sichuan, China, (b) Example of Liang Hekou Hydropower Station in Sichuan, China

AE signal and cracking and extension of sandstone during shearing process. Zhang (2018) found that the low dominant frequency with high energy of AE signals corresponds to large-scale fracture, while the high dominant frequency with low energy corresponds to small-scale fracture by uniaxial compression test of granite. Shukla *et al*. (2013) concluded that crack initiation threshold stress is most severely changed when sandstone specimens are saturated. Moreover, Yao *et al*. (2016) quantified the percentage of the stress thresholds for crack closure, crack initiation, and crack damage of coal.

Existing research on saturated rocks mainly focus on argillaceous or macro porous rocks with high water-sensitivity, such as sandstone, while there are few studies on crack propagation of dense hard rocks. Based on the advantage of AE technology, most studies were carried out from the perspective of AE parameters analysis. However, the study on fracture process of dry and saturated hard rocks based on waveform-based analysis, in particular, statistical analysis of the dominant frequency characteristics of AE waveforms, is still in its infancy.

The objective of this paper is to present the fracture evolution process of dry and saturated marble under uniaxial compression, and comprehensively discuss its difference. For this purpose, the key stress points were determined by proper methods, and dominant frequencies and amplitude of AE waveform signals in the vicinity of key points were obtained through an improved processing method. Furthermore, feature evolution of dominant frequency of AE waveforms under uniaxial compression was analyzed, and the effects of water on rock's fracture process were revealed.

2. Experimental Process and Results

2.1 Rock Samples

White marble used for the test, was taken from Baoxing in southwestern China. Its mineral composition was determined by X- ray diffractometer test. Results show that mineral calcite reached above 99.9%, which indicated that it has a single component and can exclude the influence of other factors, such as clay mineral, and stress corrosion.

The method of wet drilling was used to obtain cylindrical samples with required dimensions of $\Phi 50 \times H100$ mm in accordance with the suggested specification. To reduce the individual difference, all samples were extracted from a single marble block which has high geometrical integrity and petrographic uniformity. Both ends of the samples were ground to achieve parallel, flat, and smooth surfaces to ensure a uniform load distribution as shown in Fig. 2(b). These samples were divided into two groups, testing Group 1 for dry specimens, consisting of D1, D2, D3, D4 and testing Group 2 for saturated specimens, consisting of D5, D6, D7, D8. Dry specimens were obtained by taking into a 105°C oven more than 48 h, saturated specimens were prepared by using the method of vacuum forced saturation for 8 h and static for 4 h. To ensure the specimens obtained meets the test requirements, the degree of water saturation of two specimens, including one dry and one saturated, was measured and found its value were close to 0 and 1, respectively. The basic parameters of samples are listed in Table 1. The results of wave velocity and mineral composition tests showed that all of specimens are relatively homogeneous without obvious defects.

2.2 Experimental Setup and Equipment

A rock mechanics test system (Model: MTS815 Flex Test GT, Fig. 2(a)) was employed for the uniaxial compression tests. The capacity of the axial load transducer was 1000 kN. Loading rate was kept constant at 20 kN/min. The linear variable differential transformer (LVDT) and extensometer were used to measure the axial and ring displacement respectively.

The AE data was captured automatically by a three-dimensional real-time monitoring system (Model: PCI-2, Fig. 2(b)). Eight micro30 sensors, which have a good frequency response as well as sensitivity to AE data even in the presence of high background noise, were installed symmetrically in the radial direction along

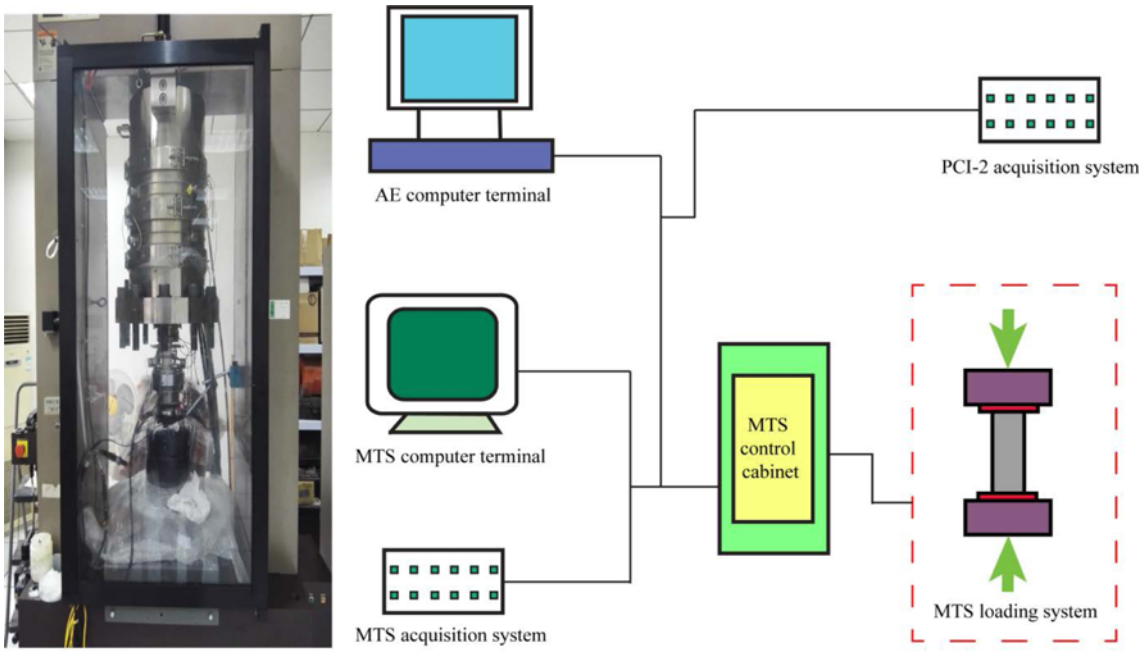

Fig. 2. The Experimental Setup: (a) MTS Loading System, (b) Schematic Diagram of Experimental System

Table 1. Basic Parameters of Marble Specimens for Uniaxial Compression Test

No.	condition	Mass M_{nat} (g)	Density ρ_{dry} ($g \cdot cm^{-3}$)	Mass M_{sat} (g) or M_{dry} (g)	P-wave velocity (m/s)	S-wave velocity (m/s)
D1	Dry	543.26	2.68	539.80	4,276.12	2,545.78
D2		540.83	2.68	536.42	4,234.69	2,734.87
D3		543.59	2.69	540.17	4,383.15	2,863.56
D4		543.19	2.69	538.79	4,396.13	2,534.45
Average		542.72	2.69	538.80	4,322.52	2,669.67
D5	Saturated	542.59	2.68	556.78	4,883.25	3,156.05
D6		542.53	2.68	553.64	4,682.50	3,169.83
D7		543.69	2.69	553.81	4,655.67	3,200.15
D8		543.73	2.69	554.85	4,597.84	3,017.66
Average		543.14	2.69	554.77	4,704.82	3,135.92

The subscript dry represents the dry state, nat represents the natural state, and sat represents the saturated state.

the surface of the cylinder, as shown in Fig. 3(a). The sampling rate of the sensors is set as 1 MHz, and the pre-amplification is 40 dB. Vaseline was used between each rock specimens and the AE sensors to guarantee good connections.

At the beginning of the test, the loading system and the AE monitoring system were started to realize the AE signal data and mechanical data monitoring and recording at the same time throughout the loading process.

2.3 Experimental Results

As shown in Fig. 4, the uniaxial compression strength (UCS) on average decreased by around 19.15%. Moreover, the elastic modulus decreased by around 35.10% averagely. This indicates that marble using in this study has strong properties of water deterioration, which is conducive to studying the water effects on fracture process.

Figure 5 shows typical failure patterns of dry and saturated specimens. Dry rock specimens mostly presented single slope shear failure. During loading application, powder debris fell at the upper end of specimen firstly, and blocky debris popped out at the same time. Then the top cracks cut through along ramp and form the domain fracture plane. However, saturated rock specimens' failure modes are relatively complex. Failure patterns with combination of shear and tensile splitting mostly were found.

3. Identification of Key Points

3.1 Methods for Identifying Key Points

The stress-strain curve is divided into four stages according to the activity states of micro-cracks under different stress levels (Cai *et al*., 2004; Bieniawski, 1967a, 1967b), as shown in Fig. 6, stage I: compression of crack closure phase, stage II: linear

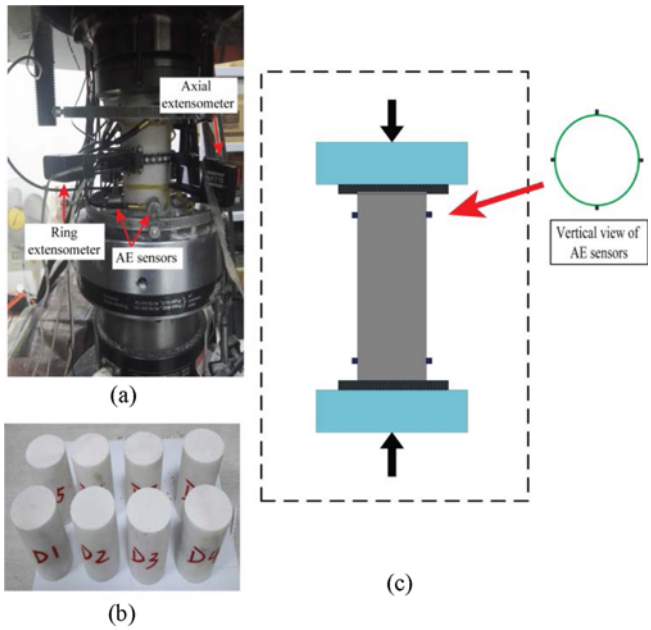

Fig. 3. Processed Rock Specimens and Its Layout before Test: (a) Specimens with Array of Sensors and Extensometers (Front View), (b) Processed Rock Specimens, (c) Schematic Diagram of Loading

elastic phase, stage III: stable crack growth phase, stage IV: unstable crack growth phase. The end points of each phase corresponding crack closure stress σ_{cc} (point *A*), crack initiation stress σ_{ci} (point *B*), damage stress σ_{cd} (point *C*)and peak stress σ_f (point *D*), which are named as "key points" of stress under uniaxial compression in this paper.

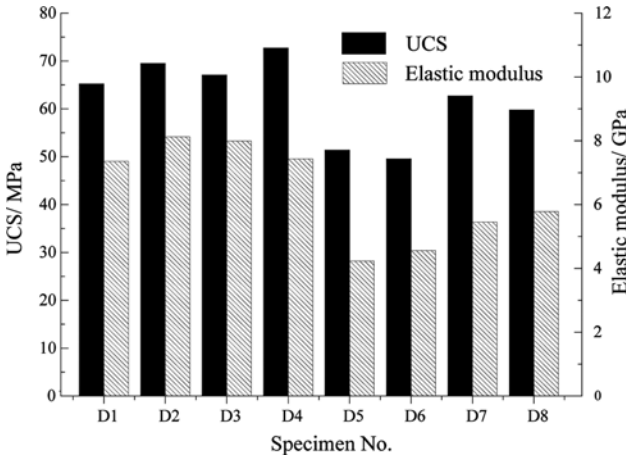

Fig. 4. UCS and Elastic Modulus of All Samples

Peak stress is distinguishable and easy to be determined. Many scholars, who have conducted a lot of studies on the other three stress values, are generally believed that closure stress can be determined by stress-strain curves. Furthermore, various methods have been proposed for identifying crack initiation and damage stress in laboratory tests, mainly including stress-strain curves method, the volumetric strain method, AE method, the stiffness of volumetric strain method. The methods of volumetric strain

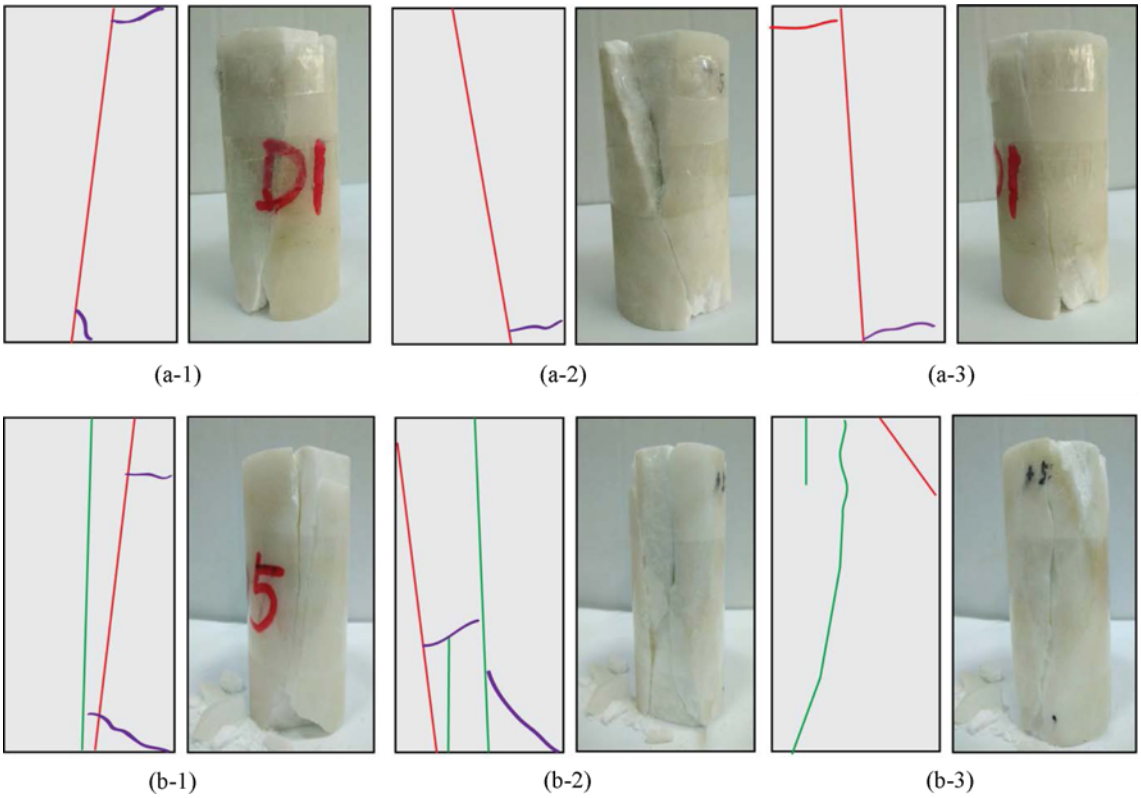

Fig. 5. Schematic Diagram of Fracture Morphology from Different Perspectives: (a-1), (a-2), and (a-3) for Dry Sample D1, (b-1), (b-2), and (b-3) for Saturated Sample D5

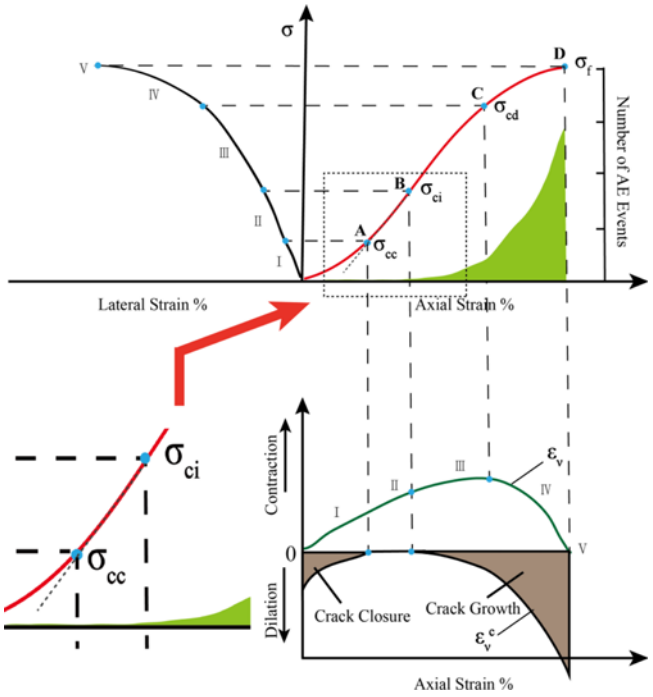

Fig. 6. Stress-Strain Diagram of a Sample Showing the Stages of Crack Development

and crack volumetric strain are more convenient and accurate, while stiffness of volumetric strain method's accuracy depends on the interval of data. AE method has greater randomness and is not widely used (Zhou *et al*., 2014; Eberhardt *et al*., 1999).

Methods for identifying these key point stresses in this paper are illustrated as follows.

1. Crack closure stress σ_{cc}. It is the end point of crack closure and also the beginning point of elastic deformation in rocks. As shown in the magnified part of Fig. 6, a line that coincides with the elastic section of the stress-strain curve is made, and the corresponding stress at the bifurcation point is the crack closure stress.
2. Crack initiation stress σ_{ci} and damage stress σ_{cd}.

σ_{ci} and σ_{cd} can be determined by various methods shown in Fig. 6. It is found the fact that, σ_{ci} is determined by the end point of the horizontal line segment of crack volumetric strain curve and σ_{cd} is determined by the inflection point of volumetric strain curve, which can avoid the subjective arbitrariness of judgment and improve the accuracy.

Martin *et al*. (1993) proposed that crack volumetric strain could be obtained by the following calculation formula

$$\varepsilon_v^c = \varepsilon_v - \varepsilon_v^e = \varepsilon_v - \frac{(1-2\mu)}{E}\sigma \tag{1}$$

where σ is the axial stress, E, μ are elastic modulus and Poisson's ratio of elastic section of stress-strain curves, ε_v, ε_v^c, ε_v^e are actual volumetric strain, crack volumetric strain, and elastic volumetric strain respectively, ε_v is calculated by the following formula:

$$\varepsilon_v = \varepsilon_1 + 2\varepsilon_3 \tag{2}$$

Where ε_1 is axial strain, ε_3 is lateral strain.

Based on formulas above, the volumetric strain and crack volumetric strain of rocks can be calculated.

3. Peak stress σ_f. The point of peak stress can be determined by experimental mechanical data.

3.2 Process of Identification

Taking dry specimen D1 and saturated specimen D5 as examples to illustrate the process of key points' identification.

As shown in Fig. 7(a), a superposition line is drawn along the elastic line segment of stress-strain curve (the red dashed line, the same below), and the corresponding stress at the bifurcation point *A* is the crack closure stress σ_{cc}, whose value is 6.48 MPa and the corresponding time is 36.1098 s. The point *D* of peak stress can be found through mechanical data table, with a value of 65.2 MPa and corresponding time is 392.0083 s.

As shown in Fig. 7(b), crack volumetric strain curve remains

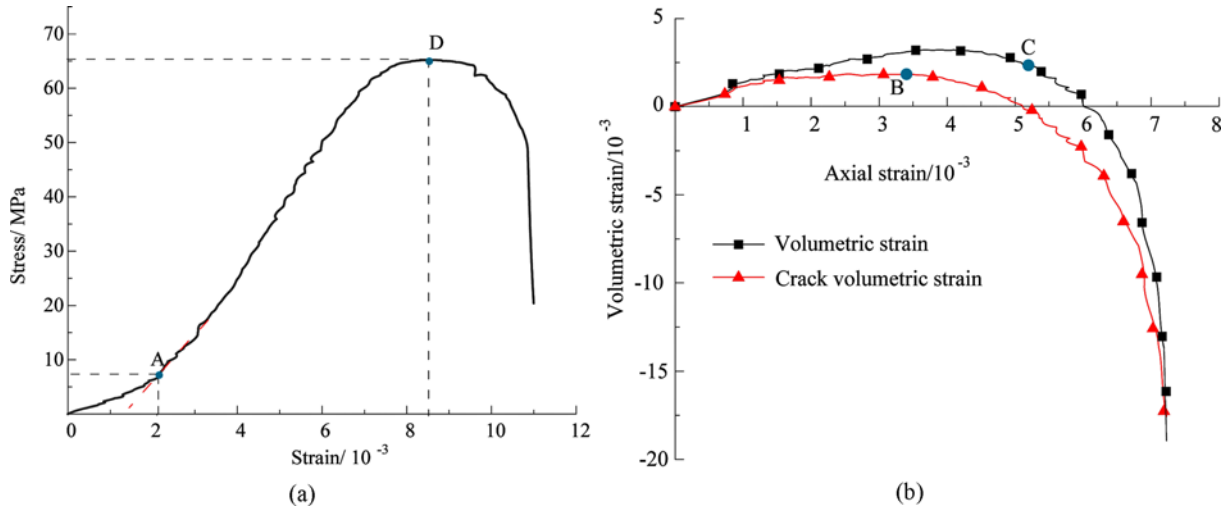

Fig. 7. Determination of Key Points of: (a) *A* and *D*, (b) *B* and *C* for Dry Specimen D1

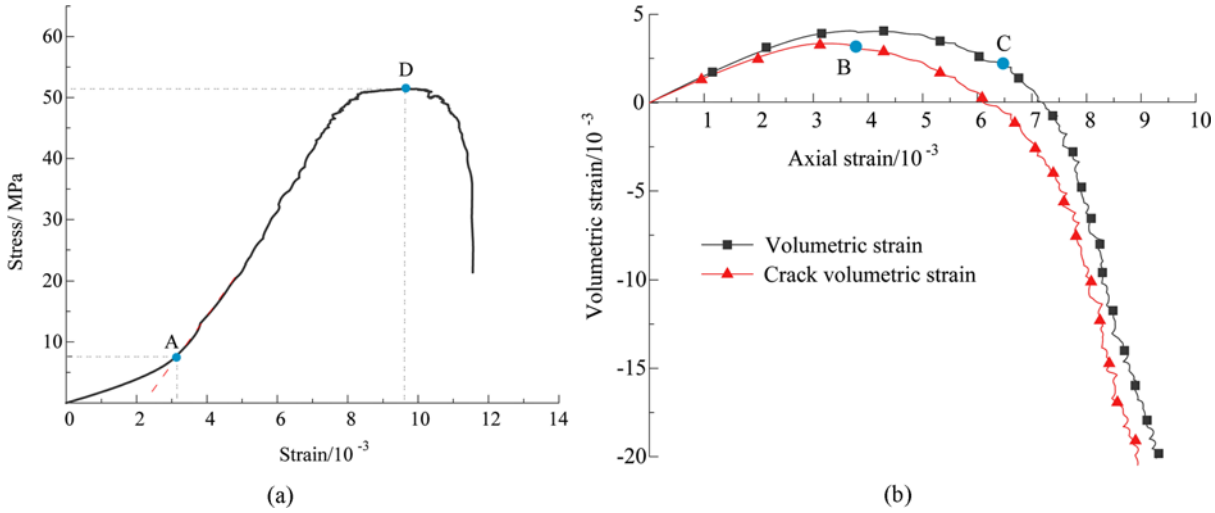

Fig. 8. Determination of Key Points of: (a) *A* and *D*, (b) *B* and *C* for Saturated Specimen D5

horizontal at the beginning, and then drops after point *B*, which is correspond to the time of crack volumetric strain increased. Stress obtained by mechanics data is 17.65 MPa, and corresponding time is 103.6965 s. Crack damage stress at the inflexion point *C* found in volumetric strain curve is 41.65 MPa and the corresponding time is 248.9346 s.

For saturated specimen D5, its crack closure stress is 7.72 MPa, corresponding time is 45.2339 s, while peak stress is 52.9 MPa, and its corresponding time is 310.5535 s, as shown in Fig. 8(a). Moreover, the crack initiation stress (point *B*) is 13.06 MPa, crack damage stress (point *C*) is 37.45 MPa, and corresponding time are 77.6638 s and 225.3223 s, respectively.

4. Analysis of Fracture Process based on Dominant Frequency Statistics

4.1 Data Processing

AE signals generated during rock test are non-stationary, and Fast Fourier transform (FFT) is a classical method of spectral analysis for it. FFT can realize effective transformation of AE waveforms from time domain to frequency domain.

AE waveform No. 5000 of sample D1 was taken as an example to illustrate extraction process of dominant frequency. With the help of MATLAB software, FFT was carried out, and two-dimensional spectrum diagram shown in Fig. 9 was obtained. Jia (2013) defined the dominant frequency as the frequency corresponding to maximum amplitude. The dominant frequency is 153 kHz and its amplitude is 0.0156 V.

4.2 Feature Evolution of Dominant Frequency During Whole Process of Compression

As shown in Figs. 10 and 11, there are lots of AE waveforms in the whole process of uniaxial compression loading. Among them, the AE waveforms sum of dry rock is more than that of the saturated. Moreover, compared with saturated rock, it takes longer for dry rock to reach peak stress.

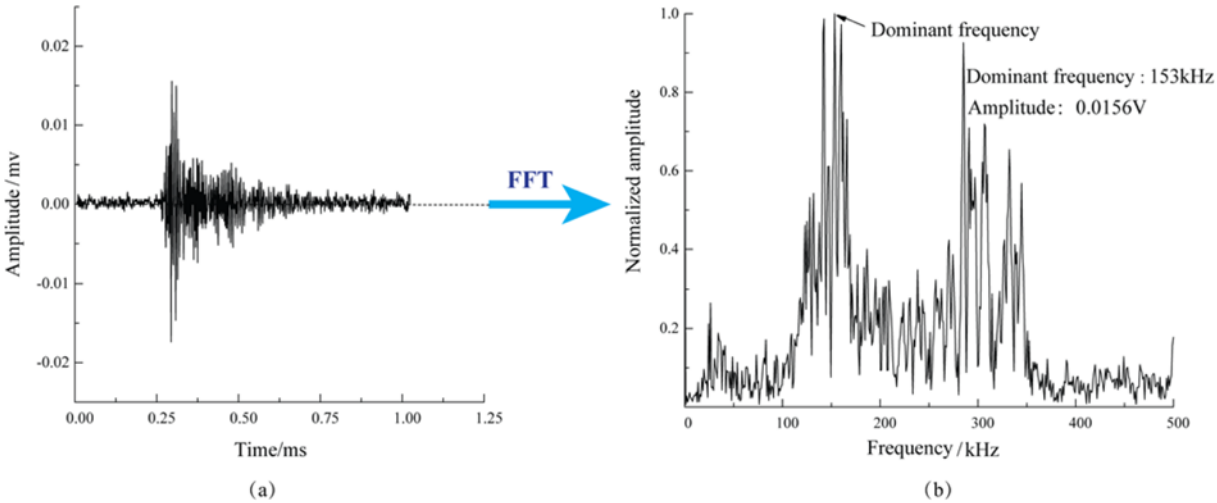

Fig. 9. Typical AE Waveform and Its Spectrum: (a) The Original AE Signal, (b) Spectrum Map

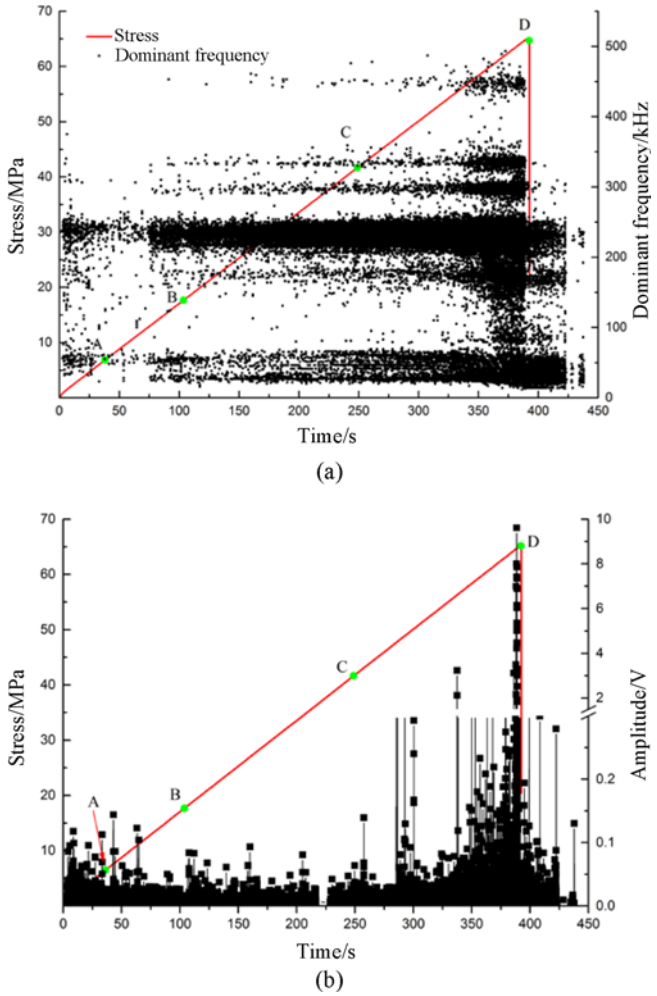

Fig. 10. The Relation Curves of: (a) Stress, Dominant Frequency versus Time, (b) Stress, Amplitude versus Time for Dry Sample D1

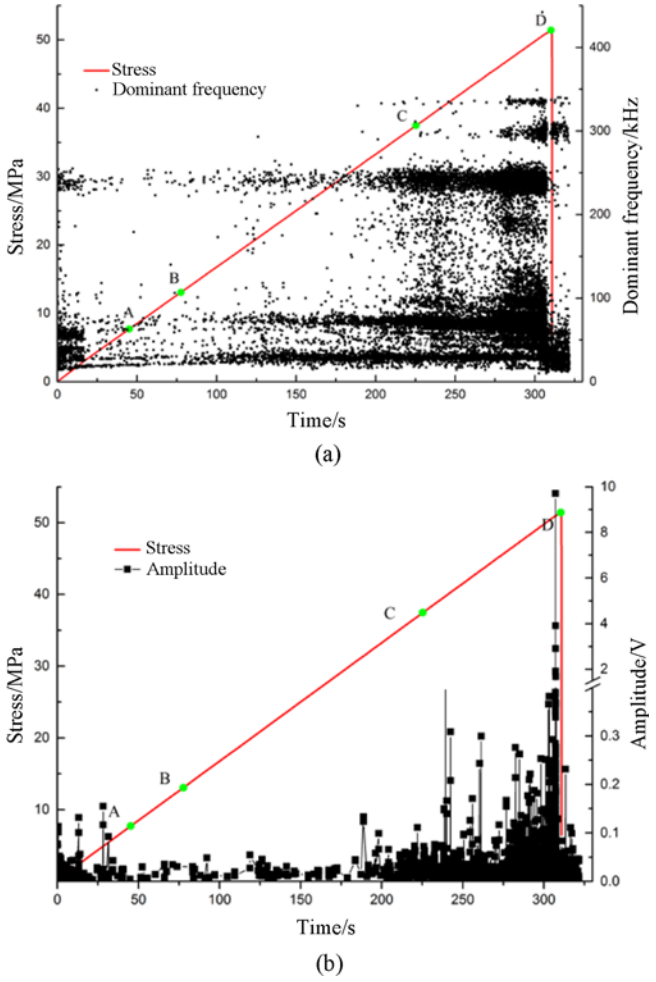

Fig. 11. The Relation Curves of: (a) Stress, Dominant Frequency versus Time, (b) Stress, Amplitude versus Time for Saturated Sample D5

The dominant frequencies of AE waveforms were divided into 46 bands. The first 45 bands have a range of 10 kHz, and those beyond 450 kHz were included in No. 46 band. It can be seen that there are two concentrations of dominant frequency bands in both dry and saturated samples, named the low dominant frequency band (L-type band) and high dominant frequency band (H-type band). The ranges of two dominant frequency bands for dry sample D1 are approximately 20 – 80 kHz and 210 – 260 kHz, and those for saturated sample D5 are 10 – 100 kHz and 180 – 300 kHz. The ranges of dominant frequency bands of saturated samples seem wider.

In the stage of crack closure, there are a certain number of AE waveforms for dry and saturated rock, and a few of them appeared with high amplitude, which reflects the closure of original defects of rock. In contrast, AE waveforms sum for dry rock is more and its amplitude is higher. In the elastic stage, AE waveforms sum and its amplitude have been kept at a low level.

In the crack unstable growth stage, the AE waveforms sum and dominant frequencies with high amplitude increased sharply. Meanwhile, dominant frequencies with low amplitude did not decrease, indicating that micro-cracks inside rock converged and connected to form macro fissures, and a large amount of energy was released centrally. After the peak strength, its amplitude decreases.

In generally, the AE waveforms energy for dry rock, which corresponds to the amplitude, is higher than that of saturated rock. The intensity of crack fusion, expansion, penetration of saturated rock is weaker. Moreover, the elastic modulus and AE waveforms sum decrease after saturation described in Figs. 4 and 11(a), respectively. It can be concluded that water enhances the ductility and creep characteristics of rock.

4.3 Feature Evolution of Dominant Frequency of Key Points

To explore the water effects on characteristics of AE waveform signals, the dominant frequencies of AE waveforms in the vicinity of each key point are analyzed through statistical methods. As the data of AE and mechanical is recorded at the same time in the entire test, the corresponding waveform data file of events which happened at the time of key points can be found. Then dominant frequency and its amplitude can be

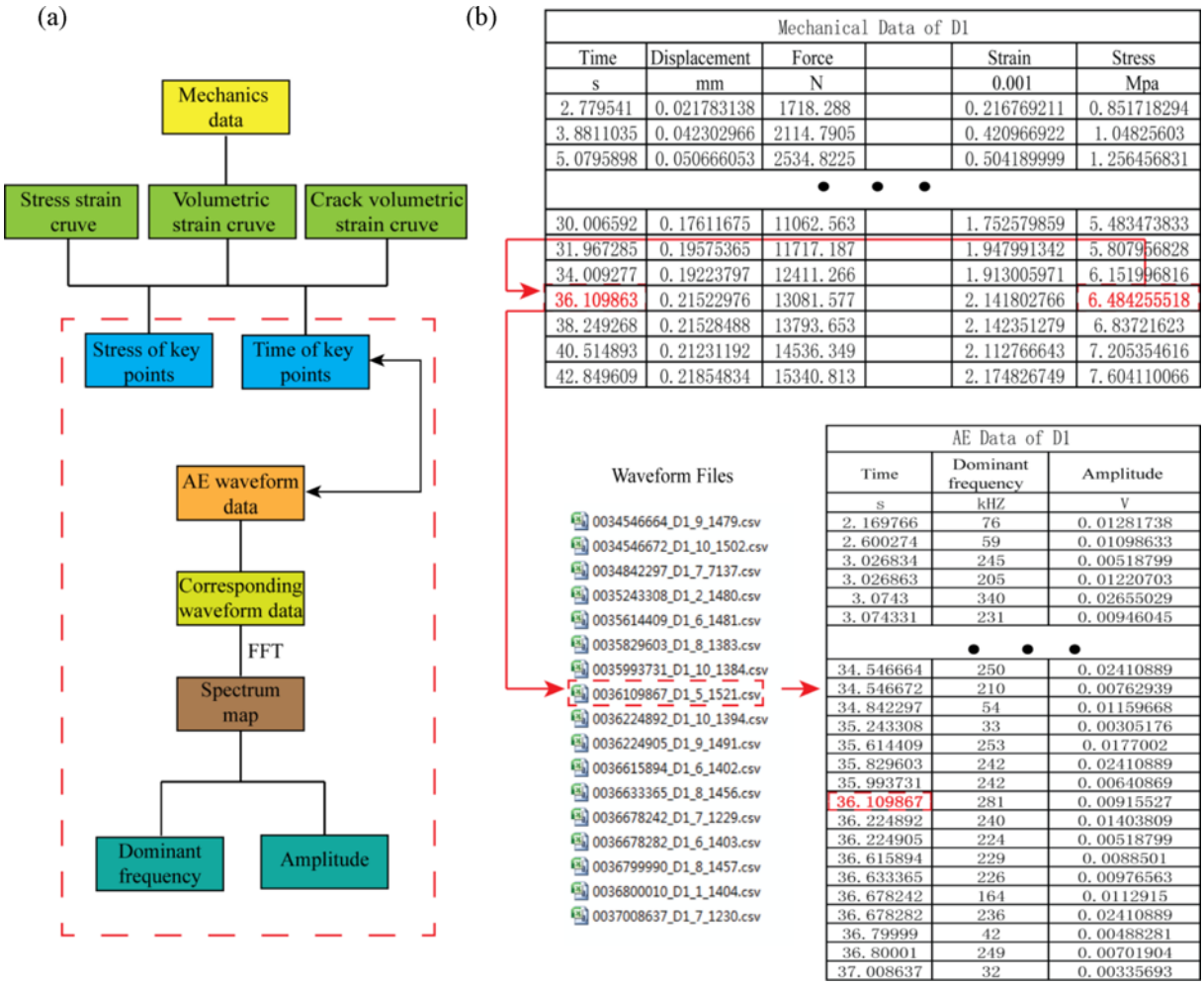

Fig. 12. Process of Dominant Frequency Extraction: (a) The Whole Flow Diagram, (b) Example of Dominant Frequency Extraction for Dry Sample D1 in the Vicinity of Point A

Table 2. Statistics of Waveforms Sum and Proportions of High and Low Dominant Frequency Bands in the Vicinity of Key Points

No.	Condition	Point A			Point B			Point C			Point D		
		Waveforms sum	Proportion of frequency bands (%)		Waveforms sum	Proportion of frequency bands (%)		Waveforms sum	Proportion of frequency bands (%)		Waveforms sum	Proportion of frequency bands (%)	
			H-type	L-type		H-type	L-type		H-type	L-type		H-type	L-type
D1	Dry	367	77.61	16.42	1,654	94.74	1.58	1,190	84.48	11.11	3,571	24.52	71.28
D2		989	56.61	39.68	2,511	68.69	27.98	4,259	52.91	45.72	6,693	21.89	73.6
D3		417	58.82	38.18	1,415	74.78	23.24	3,765	54.78	40.87	5,120	19.39	74.69
D4		958	97.7	2.15	963	93.33	6.67	3,113	54.51	44.01	6,092	27.17	70.81
Average		683	72.69	24.11	1,635	82.86	14.87	3,082	61.67	35.43	5,369	23.24	72.60
D5	Saturated	264	3.02	96.88	306	27.14	66.67	2,146	21.74	78.26	3,155	9	86.58
D6		424	12.5	83.33	230	34.82	60.18	3,384	6.67	80	3,888	29.35	69.6
D7		311	18.18	81.82	297	22.22	77.78	3,925	4.46	94.64	6,928	18.46	78.72
D8		249	8.72	91.28	244	13.21	86.09	2,854	3.28	96.72	3,498	10.83	88.91
Average		312	10.61	88.33	269	24.35	72.68	3,077	9.04	87.41	4,367	16.91	80.95

extracted through FFT method. The process is shown in Fig. 12.

Considering the accuracy of key points identified above and the validity of statistics, the dominant frequencies at the moment of each key point and within the previous 10s is selected for analysis. The proportions of H-type and L-type bands in the vicinity of each key point of all samples are calculated as shown in Table 2. Moreover, the proportions of H-type bands for all samples are shown in Fig. 13, and proportion of L-type is negatively correlated with it.

As shown in Table 2, the average numbers of point *A* and point

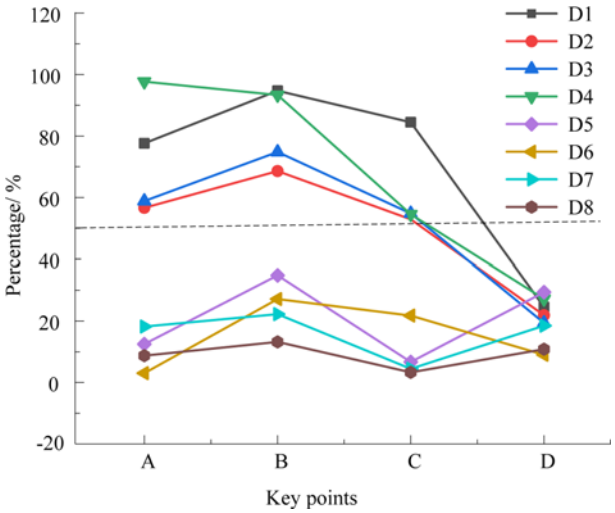

Fig. 13. Proportions of H-type Waveforms in the Vicinity of Key Points

B are over 300 and 250, while those for point C and point D are over 3,000 and 4,300, respectively. It is concluded that the statistical numbers meets the requirements and can reflect regularity accurately. As the loading continues, the AE waveforms sum increased. Moreover, the average AE waveforms sum of saturated rock is less than that of dry rock in the vicinity of all key points.

The proportions of H-type bands for dry rock account for 72.69%, 82.86%, 61.67%, 23.24% on average compared with 24.11%, 14.87%, 35.43%, 72.60% for L-type bands at points *A*, *B*, *C*, and *D*. Compared to dry rock, the proportions of H-type waveforms observed decrease to 10.61%, 24.35%, 9.04%, 16.91% on average for saturated rock in the vicinity of each key point, whereas the proportions of L-type bands increase to 88.33%, 72.68%, 87.41%, 80.95%, respectively. The results show that, for dry rock, the proportions of H-type waveforms are higher than that of L-type waveforms at points *A*, *B* and *C*, while it turns out to be the opposite at point *D*. For saturated rock, the proportions of H-type waveforms are lower than that of L-type waveforms at each key point. It also reveals that marble specimens exhibit characteristic of L-type at point *D*, and its proportion of saturated rock is higher than that of dry rock.

As shown in Fig. 13, the proportions of H-type bands of dry rock increase on the whole from point *A* to point *B*, and decrease from point *B* to point *C*. Moreover, it decreases significantly at point *D*, which is lower than proportion of L-type band. Compared to dry rock, the proportions of H-type bands for saturated rock increase from point *A* to point *B*, then decrease from point *B* to point *C*, while it increase at point *D*. In addition, the results of proportions of dominant frequency bands for saturated rock in the vicinity of each key point show less dispersion.

5. Discussions

Cai *et al*. (2007a) pointed out that AE waveforms of high frequency correspond to small-scale fracture and the low frequency correspond to large fracture. Deng *et al*. (2018) and Li *et al.* (2017) found that H-type waveforms are produced by micro-shear failure and L-type waveforms are caused by micro-tensile failure through statistical analysis of different rocks under different loading conditions. For rock under natural condition, Deng *et al*. (2018) proposed that micro-shear failures play dominant role for rock fracture under compression. So same as dry rock in this study, abundant of high dominant frequencies, corresponding to micro-shear failures, can also be observed as shown in Fig. 10(a). For dry rock, micro-shear failures are dominant in the stage of crack closure, stable and unstable crack propagation, and the shear failure plane is formed. After reaching point *C* (crack damage stress), micro-tensile failures occurred along with micro-shear failures, and were to be dominant. This observation shed light on us that appearance of a large number of low dominant frequencies is the precursor information of violent activity of cracks and imminent failure of dry rock.

Compared to dry rock, the proportions of L-type AE waveforms for saturated rock increased in the vicinity of each key point. It implies that the effects of water increased the number of micro-tensile failures at the key moment of crack propagation and resulted in macro tensile fracture morphology, which is consistent with phenomenon mentioned in section 2.3 above.

In the vicinity of point *A* and point *B*, AE signals with high dominant frequencies for dry rock mainly were produced, while saturated rock generated the ones with low dominant frequencies. This may result from that, the large-scale micro failures for dry and saturated rock decrease in elastic stage, and the proportions of L-type waveforms decrease. The cracks' activity of dry rock was more intense, and AE waveforms sum increased. Whereas, due to the existence of water, AE waveforms sum of saturated rock decreases relatively (Table 2). From point *B* to point *C*, accompanied by large-scale failures, cracks inside rock experienced from stable to unstable propagation stages, thus the proportions of H-type waveforms for dry and saturated rock decrease. At peak stress (point *D*), the number of large-scale failures of the dry has increased dramatically, resulting in reduction of percentage of H-type waveforms. While the effect of water bringing about more micro-tensile failure is weakened, proportion of L-type waveforms for saturated rock decreased. Based on the above analysis, it can be concluded that the role of water in increasing micro-tensile failures is most obvious at point *C*.

6. Conclusions

Based on this research, the following conclusions presented hereinafter can be obtained. During the whole process of uniaxial compression test, AE waveform signals with high dominant frequency and amplitude rarely can be found in the crack closure stage. At elastic stage, its amplitude starts to decrease. From the unstable stage of crack growth to peak stress, a mount of AE waveform signals with high dominant frequency and amplitude exist. There are two concentrations of dominant frequency bands

in both dry and saturated marble, and the ranges of dominant frequency bands of the saturated seem wider than the dry ones. Compared to dry rock, AE waveform sum for the saturated is fewer and its amplitude of dominant frequency is lower, indicating that water enhances the ductility and creep characteristics of rock.

The proportions of H-type bands for dry rock are higher than proportions of L-type bands at point *A*, point *B* and point *C*, while saturated rock's situation is opposite. At point *D*, the proportions of H-type bands of dry rock and saturated rock are lower than L-type bands, and the proportion of L-type band of dry rock is lower than saturated rock. It reveals that appearance of lots of waveforms signals with low dominant frequency is the precursor information of violent activity of cracks and failure for dry rock, and the effects of water increased the number of micro-tensile failure for saturated rock in the vicinity of each key point.

From point *A*, point *B*, point *C* to point *D*, the proportions of H-type bands in the vicinity of key points for dry rock show a trend of increasing - decreasing - sharply decreasing, while those for saturated rock follow the law of increasing - decreasing - increasing.

Acknowledgements

This work was supported by the National Natural Science Foundation of China (Grant No. 41772322) and the National Key Research and Development Program of China (Grant No. 2016YFC0600702). The authors also thank the editors and anonymous reviewers for their constructive comments that improved the manuscript.

References

Areias, P., Reinoso, J., Camanho, P., and Rabczuk, T. (2015). "A constitutive-based element-by-element crack propagation algorithm with local mesh refinement." *Computational Mechanics*, Vol. 56, pp. 291-315, DOI: 10.1007/s00466-015-1172-z.

Areias, P., Reinoso, J., Camanho, P., Césarde Sá, J. C., and Rabczuk, T. (2018). "Effective 2d and 3d crack propagation with local mesh refinement and the screened Poisson equation." *Engineering Fracture Mechanics*, Vol. 189, pp. 339-360, DOI: 10.1016/j.engfracmech.2017.11.017.

Bieniawski, Z. T. (1967a). "Mechanism of brittle fracture of rock: Part I — theory of the fracture process." *International Journal of Rock Mechanics & Mining Sciences & Geo-mechanics Abstracts,* Vol. 4, No. 4, pp. 395, IN11, 405-404, IN12, 406, DOI: 10.1016/0148-9062(67)90030-7.

Bieniawski, Z. T. (1967b). "Mechanism of brittle rock fracture: Part II — experimental studies." *International Journal of Rock Mechanics & Mining Sciences,* Vol. 4, No. 4, pp. 407-423, DOI: 10.1016/0148-9062(67)90031-9.

Cai, M., Kaiser, P. K., Morioka, H., Minami, M., Maejima, T., Tasaka, Y., and Kurose, H. (2007a). "FLAC/PFC coupled numerical simulation of AE in large-scale underground excavations." *International Journal of Rock Mechanics & Mining Sciences*, Vol. 44, No. 4, pp. 550-564, DOI: 10.1016/j.ijrmms.2006.09.013.

Cai, M., Kaiser, P. K., Tasaka, Y., Maejima, T., Kurose, H., and Minami, M. (2004) "Generalized crack initiation and crack damage stress thresholds of brittle rock masses near underground excavations." *International Journal of Rock Mechanics & Mining Sciences*, Vol. 41, No. 5, pp. 833-847, DOI: 10.1016/j.ijrmms.2004.02.001.

Cai, M., Morioka, H., Kaiser, P. K., Tasaka, Y., Kur-ose, H., Minami, M., and Maejima, T. (2007b). "Back-analysis of rock mass strength parameters using AE monitoring data." *International Journal of Rock Mechanics & Mining Sciences*, Vol. 44, No. 4, pp. 538-549, DOI: 10.1016/j.ijrmms.2006.09.012.

Deng, J. H., Li, L. R., Chen, F., Liu, J. F., and Yu, J. (2018). "Twin-peak frequencies of acoustic emission due to the fracture of marble and their possible mechanism." *Advanced Engineering Sciences,* Vol. 50, No. 5, pp. 1-6.

Eberhardt, E., Stead, D., and Stimpson, B. (1999). "Quantifying progressive pre-peak brittle fracture damage in rock during uniaxial compression." *International Journal of Rock Mechanics & Mining Sciences,* Vol. 36, No. 3, pp. 361-380. DOI: 10.1016/S0148-9062(99)00019-4.

Eberhardt, E., Stead, D., Stimpson, B., and Read, R. S. (1998). "Identifying crack initiation and propagation thresholds in brittle rock." *Canadian Geotechnical Journal*, Vol. 35, No. 2, pp. 222-233, DOI: 10.1139/cgj-35-2-222.

Erguler, Z. A. and Ulusay, R. (2009). "Water-induced variations in mechanical properties of clay-bearing rocks." *International Journal of Rock Mechanics & Mining Sciences,* Vol. 46, No. 2, pp. 355-370, DOI: 10.1016/j.ijrmms.2008.07.002.

Hawkins, A. B. and Mcconnell, B. J. (1992). "Sensitivity of sandstone strength and deformability to changes in moisture content." *Quarterly Journal of Engineering Geology and Hydrogeology,* Vol. 25, No. 2, pp. 115-130, DOI: 10.1144/gsl.qjeg.1992.025.02.05.

Jia, X. N. (2013). *Experimental study on acoustic emission Eigen-frequency spectrum features of strain bursts,* PhD Thesis, China University of Mining and Technology, Beijing, China.

Khazaei, C., Hazzard, J., and Chalaturnyk, R. (2015). "Damage quantification of intact rocks using acoustic emission energies recorded during uniaxial compression test and discrete element modeling." *Computers & Geotechnics,* Vol. 67, pp. 94-102, DOI: 10.1016/j.compgeo.2015.02.012.

Li, L. R., Deng, J. H., Zheng, L., and Liu, J. F. (2017). "Dominant frequency characteristics of acoustic emissions in white marble during direct tensile tests." *Rock Mechanics & Rock Engineering,* Vol. 50, No. 5, pp. 1-10. DOI: 10.1007/s00603-016-1162-2.

Lu, C. P., Dou, L. M., Liu, H., Liu, H. S., Liu, B., and Du, B. B. (2012). "Case study on micro seismic effect of coal and gas outburst process." *International Journal of Rock Mechanics & Mining Sciences*, Vol. 53, No. 53, pp. 101-110. DOI: 10.1016/j.ijrmms.2012.05.009.

Martin, C. D. (1993). *The strength of massive Lac du Bonnet granite around underground opening,* PhD thesis, University of Manitoba, Winnipeg ,Canada.

Rabczuk, T., Areias, P., and Belytschko, T. (2007). "A meshfree thin shell method for nonlinear dynamic fracture," *International Journal for Numerical Methods in Engineering*, Vol. 72, pp. 524-548, DOI: 10.1002/nme. 2013.

Ren, H., Zhuang, X. Y., Cai, Y., and Rabczuk, T. (2016). "Dual-horizon peridynamics." *International Journal for Numerical Methods in Engineering*, Vol. 108, pp. 1451-1476, DOI: 10.1002/nme.5257.

Rodríguez, P., Arab, P. B., and Celestino, T. B. (2016). "Characterization of rock cracking patterns in diametral compression tests by acoustic emission and petrographic analysis." *International Journal of Rock Mechanics & Mining Sciences*, Vol. 83, pp. 73-85, DOI: 10.1016/

j.ijrmms.2015.12.017.

Shukla, R., Ranjith, P. G., Choi, S. K., and Haque, A. (2013). "Mechanical behaviour of reservoir rock under brine saturation." *Rock Mechanics & Rock Engineering*, Vol. 46, No. 1, pp. 83-93, DOI: 10.1007/s00603-012-0246-x.

Wang, X., Wen, Z., Jiang, Y., and Huang, H. (2018). "Experimental study on mechanical and acoustic emission characteristics of rock-like material under non-uniformly distributed loads." *Rock Mechanics & Rock Engineering*, 2018, Vol. 51, No. 3, pp. 1-17, DOI: 10.1007/s00603-017-1363-3.

Wu, J. Y. (2018). "A geometrically regularized gradient-damage model with energetic equivalence." *Computer Methods in Applied Mechanics and Engineering,* Vol. 328, pp. 612-637, DOI: 10.1016/j.cma.2017.09.027.

Xiong, D. G., Zhao, Z. M., Su, C. D., and Wang, G. Y. (2011). "Experimental study of effect of water-saturated state onmechanical properties of rock in coal measure strata." *Chinese Journal of Rock Mechanics and Engineering*, Vol. 30, No. 5, pp. 998-1006, DOI: 10.1631/jzus.B1000185.

Xu, J., Wu, H., and Lu, L. F. Yang, H. W., and Tan, H. Y. (2012). "Experimental study of acoustic emission characteristics during shearing process of sandstone under different water contents." *Chinese Journal of Rock Mechanics & Engineering,* Vol. 31, No. 5, pp. 914-920.

Yao, Q. L., Chen, T., Ju, M., Liang, S., and Li, X. (2016). "Effects of water intrusion on mechanical properties of and crack propagation in coal." *Rock Mechanics & Rock Engineering,* Vol. 49, No. 12, pp. 1-11, DOI: 10.1007/s00603-016-1079-9.

Yilmaz (2010). "Influence of water content on the strength and deformability of gypsum." *International Journal of Rock Mechanics & Mining Sciences,* Vol. 47, No. 2, pp. 342-347, DOI: 10.1016/j.ijrmms.2009.09.002.

Zhang, J. W. (2018). "Investigation of relation between fracture scale and acoustic emission time-frequency parameters in rocks." *Shock and Vibration*, Vol. 12, pp. 1-14, DOI: 10.1155/2018/3057628.

Zhang, Y. B., Huang, X. H., Li, S. S., and Liu, X. X. (2013). "Spectral character analysis of sandstone under saturation condition in rupture procedure." *Rock and Soil Mechanics*, Vol. 34, No. 6, pp. 1574-1578, DOI: 10.1016/j.jhsa.2013.08.024.

Zhang, Y., Lackner, R., Zeiml, M., and Mang, H. (2015). "Strong discontinuity embedded approach with standard SOS formulation: Element formulation, energy-based crack-tracking strategy, and validations." *Computer Methods in Applied Mechanics and Engineering*, Vol. 287, pp. 335-366, DOI: 10.1016/j.cma.2015.02.001.

Zhang, Y. and Zhuang, X. Y. (2018). "Cracking elements: A self-propagating strong discontinuity embedded approach for quasi-brittle fracture," *Finite Elements in Analysis and Design*, Vol. 144, pp. 84-100, DOI: 10.1016/j.finel.2017.10.007.

Zhou, H., Meng, F. Z., Lu, J. J., Zhang, C. Q., and Yang, F. J. (2014). "Discussion on methods for calculating crack crack initiation strength and crack damage strength for hard rock." *Rock and Soil Mechanics*, Vol. 35, No. 4, pp. 913-918.

Zhou, S., Zhu, H. H., Ju, J. W., Yan, Z., and Chen, Q. (2017). "Modeling microcapsule-enabled self-healing cementitious composite materials using discrete element method." *International Journal of Damage Mechanics*, Vol. 26, No. 2, pp. 340-357, DOI: 10.1177/1056789516688835.

Zhou, S., Zhu, H. H., Yan, Z., Ju, J. W., and Zhang, L. (2016). "A micromechanical study of the breakage mechanism of microcapsules in concrete using PFC2D." *Construction and Building Materials*, Vol. 115, pp. 452-463, DOI: 10.1016/j.conbuildmat.2016. 04.067.

Zhu, H. H., Zhou, S., Yan, Z., Ju, J. W., and Chen, Q. (2015). "A two-dimensional micromechanical damage-healing model on micro crack-induced damage for microcapsule-enabled self-healing cementitious composites under tensile loading." *International Journal of Damage Mechanics*, Vol. 24, No. 1, pp. 95-115, https://doi.org/10.1177/1056789514522503.